All-optical production of 6Li quantum gases

Author(s):
Burchianti, Alessia; Seman, Jorge A.; Valtolina, Giacomo; Morales, Andrea; Inguscio, Massimo; Zaccanti, Matteo; Roati, Giacomo

Publication date:
2015

Permanent link:
https://doi.org/10.3929/ethz-b-000100686

Originally published in:
Journal of Physics: Conference Series 594(1), https://doi.org/10.1088/1742-6596/594/1/012042

All-optical production of ^{6}Li quantum gases

All-optical production of ^{6}Li quantum gases

A Burchianti[1,2], J A Seman[1,2,3], G Valtolina[1,2,4], A Morales[5], M Inguscio[2,6], M Zaccanti[1,2] and G Roati[1,2]

[1]INO-CNR, via Nello Carrara 1, 50019 Sesto Fiorentino, Italy
[2]LENS and Università di Firenze, Via Nello Carrara 1, 50019 Sesto Fiorentino, Italy
[4]Scuola Normale Superiore, Piazza dei Cavalieri, 7, 56126 Pisa, Italy
[5]Department of Physics, ETH Zürich, 8093 Zürich, Switzerland
[6]INRIM, Strada delle Cacce 91, 10135 Torino, Italy

E-mail: burchianti@lens.unifi.it

Abstract. We report efficient production of quantum gases of ^{6}Li using a sub-Doppler cooling scheme based on the D_1 transition. After loading in a standard magneto-optical trap, an atomic sample of 10^9 atoms is cooled at a temperature of 40 μK by a bichromatic D_1 gray-molasses. More than 2×10^7 atoms are then transferred into a high-intensity optical dipole trap, where a two-spin state mixture is evaporatively cooled down to quantum degeneracy. We observe that D_1 cooling remains effective in the deep trapping potential, allowing an effective increase of the atomic phase-space density before starting the evaporation. In a total experimental cycle of 11 s, we produce weakly-interacting degenerate Fermi gases of 7×10^5 atoms at $T/T_F < 0.1$ and molecular Bose-Einstein condensates of up 5×10^5 molecules. We further describe a simple and compact optical system both for high-resolution imaging and for imprinting a thin optical barrier on the atomic cloud; this represents a first step towards the study of quantum tunneling in strongly interacting superfluid Fermi gases.

1. Introduction

Ultracold atoms, due to their high tunability and control, represent an ideal test ground for many-body physics [1]. In particular, the advent of ultracold atomic Fermi gases has proved the possibility to address, with unprecedented clarity, open questions in condensed matter which arise in strongly correlated electron systems [2]. Indeed, contrary to real electronic materials, dilute degenerate Fermi gases confined in optical traps offer a wealth of experimentally accessible parameters, including the interaction strength between particles, the confinement and the dimensionality. Continuous efforts have been thus devoted to the development of experimental methods for fast and efficient production of large and highly degenerate fermionic samples which are the starting point for more complex experiments. In this context, all-optical schemes are preferred to magnetic ones, due to their higher flexibility [3]. One of the main advantages is the possibility of trapping any internal state, eventually in the presence of a magnetic field. This allows the implementation of efficient forced evaporation close to a magnetically-tuned Feshbach resonance [4, 5]. The feasibility of this approach requires cold and dense atomic clouds in order to match the optical trap volume and depth. This guarantees that a large fraction of atoms is

[3] Present address: Instituto de Física, Universidad Nacional Autónoma de México, Apartado Postal 20-364, 01000 México Distrito Federal, Mexico.

transferred from the magneto-optical trap (MOT) into the optical potential, where the sample is then evaporatively cooled to quantum degeneracy.

Atomic samples at sub-Doppler temperatures are generally produced by exploiting Sisyphus cooling in optical molasses [6]. However, for lithium and potassium, which are the only alkali-metal atoms with stable fermionic isotopes, the standard Sisyphus mechanism, working on the D_2 transition, is complicated by the unresolved hyperfine splitting of the excited state. Lately, several groups have proved efficient sub-Doppler cooling of bosonic ^{7}Li and two potassium isotopes using gray-molasses [7–10], where Sisyphus cooling occurs on the blue side of D_1 transition [11–14]. Recently, following the pioneering work in Ref. [7] on ^{40}K, we have successfully extended the D_1 gray-molasses cooling technique to the case of ^{6}Li [15]. Similar results have also been reported in Ref. [16], where simultaneous sub-Doppler laser cooling of ^{6}Li and ^{40}K has been achieved using the D_1 transitions for both atomic species. We recall that atomic samples of both ^{6}Li and ^{40}K at temperatures of a few tens of μK have also been produced in MOTs, working on narrow dipole transitions lying in the near-UV region [17–19]. Despite its effectiveness, the latter method has the drawback to require special optics and quite expensive laser sources, when compared with the previous one.

In this paper, we describe sub-Doppler cooling of ^{6}Li using the D_1 transition and demonstrate how the introduction of this novel cooling stage allows for efficient production of quantum gases of ^{6}Li. After collecting an atomic ^{6}Li sample in a standard MOT, we apply bichromatic cooling in a D_1 gray-molasses. A laser field, blue-detuned from the $2S_{1/2}(F = 3/2) \rightarrow 2P_{1/2}(F' = 3/2)$ transition, produces Sisyphus cooling, while a weaker laser field allows phase-coherent addressing of the $2S_{1/2}(F = 1/2) \rightarrow 2P_{1/2}(F' = 3/2)$ transition, creating velocity-selective coherent population trapping (VSCPT), as soon as the two lasers are in Raman configuration [8]. The emergence of quantum interference at the Raman resonance provides an extra-cooling effect. After 2 ms in the D_1 molasses, the temperature of the atomic cloud drops from 500 μK to 40 μK, without any significant changes in the number of captured atoms ($\sim 10^9$ atoms). Then, more than 2×10^7 atoms are transferred into a far-detuned optical dipole trap (ODT) at 1070 nm. We observe that the D_1 cooling works even in the presence of a deep trapping potential. This implies a 40-fold increase of the phase-space density of the sample before starting the evaporation. The scattering lengths between two of the lowest spin states of ^{6}Li are magnetically tuned via their Feshbach resonance allowing us to explore both the BEC and BCS side of the resonance. As a proof of the feasibility of the developed technique, we produce, in a total cycle time of 11 s, either molecular Bose-Einstein condensates (mBECs) of 5×10^5 molecules or binary mixtures of degenerate Fermi gases of 3.5×10^5 atoms per spin state at $T/T_F < 0.1$, where T_F is the Fermi temperature. Furthermore, we discuss the realization in our setup of a simple and inexpensive optical system for both high-resolution imaging and for imprinting a thin optical barrier on the atomic sample. This repulsive potential, superimposed to the one produced by the optical trap, creates a double-well potential. We plan to use this trap geometry to investigate coherent tunneling of ^{6}Li quantum gases throughout different interaction regimes.

2. Experimental setup

Our experimental setup (see Fig. 1) consists of two main parts: the oven assembly, where a enriched ^{6}Li sample (isotopic abundance>99%) is heated at a temperature of 440°C, and the science chamber, where we perform the experiments. These two regions are connected by the Zeeman slower tube and by a differential pumping stage section. The residual pressure in the chamber is 10^{-11} Torr. The chamber is a spherical octagon with a large optical access. In particular, two reentrant CF100 viewports allow us to set up a high-resolution imaging system along the vertical direction (z-axis). The atoms from the thermal beam, slowed down by the Zeeman slower, enter in the science chamber, where they are captured by a MOT operating on D_2 ($2S_{1/2} \rightarrow 2P_{3/2}$) optical transitions (see Fig. 2). The MOT light configuration consists

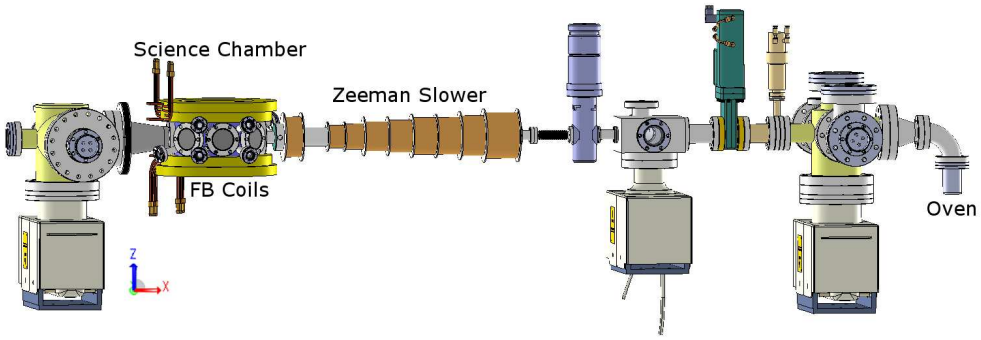

Figure 1. Sketch of the experimental setup. A thermal atomic beam is produced by evaporating a ^{6}Li sample in a oven kept at 440°C. The atoms slowed by a Zeeman slower enter inside the science chamber where they are collected by a MOT. The Feshbach (FB) coils produce a suitable magnetic field for tuning the atomic scattering length.

of three mutually orthogonal retro-reflected laser beams with circular polarization (σ^+/σ^-), crossing in the center of the chamber (see Fig. 3). The beams have a $1/e^2$ radius of about 1.5 cm, and peak intensity of about 7 I_S, where I_S=2.54 mW/cm^2 is the saturation intensity of the D_2 transition. Each beam contains both cooling (-9 Γ detuned from the F=3/2 $\rightarrow$ F'=5/2 transition, where $\Gamma = 2\pi \times 5.87$ MHz) and repumper (-6 Γ detuned from the F=1/2 $\rightarrow$ F'=3/2 transition) light. The cooling power is a factor 1.5 higher than the repumper one. In 5 s, 2×10^9 atoms are loaded into the MOT and cooled at a temperature of 2.5 mK. Then, the atomic beam, coming from the oven, is blocked with a mechanical shutter and the Zeeman slower light and magnetic field are turned off. It follows a cooling and compression phase, where the intensity and the detuning of both cooling and repumper light is reduced. After this phase lasting 2 ms, the temperature of the atomic cloud drops to 500 μK and 1.6×10^9 atoms remain trapped. At this point, we turn off the D_2 lights and the MOT magnetic quadrupole field, while turning on the D_1 molasses. The laser beams forming the D_1 molasses follow the same optical path of those of the D_2 MOT (see Fig. 3). Each beam contains the cooling (F=3/2 $\rightarrow$ F'=3/2) and repumper lights (F=1/2 $\rightarrow$ F'=3/2), both blue detuned with respect to the resonances (see Fig. 2). The maximum available peak intensity for beam is 3 I_S and the ratio between cooling and repumper power is set close to 5, the value that experimentally gives the maximum D_1 cooling efficiency. The D_2 and D_1 lights are derived from two amplified laser diodes which are controlled with two acusto-optic modulators (AOMs), acting as fast light switches. The two lasers inject the same tapered amplifiers, so the same optical components are used to realize the D_2 MOT and D_1 molasses. This scheme has the advantage that no further adjustment of the molasses alignment is needed.

During the D_1 cooling phase the atoms are transferred into a ODT consisting of one single focused laser beam derived from a 200 W multi-mode ytterbium fiber laser with a central wavelength of 1073 nm. The trapping beam forms an angle of about 15° with one of the horizontal MOT/molasses beam, as shown in Fig. 3, and it is focused on the atoms with a waist of 42 μm. In order to enlarge the spatial overlap between the molasses and the ODT, the trapping volume is increased by modulating the frequency and amplitude of the ODT's control AOM at a frequency (1.2 MHz and 600 kHz, respectively) larger than the trapping frequencies.

This produces an effective elliptic Gaussian-shaped beam with waists of about 42 μm (along the z-axis)$\times$85 μm. The initial trap power is set to 120 Watt which corresponds to a trap depth of $\sim$1.3 mK.

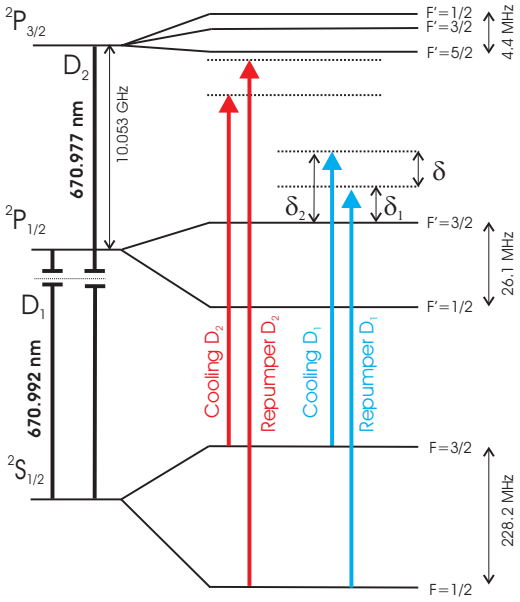

Figure 2. ^{6}Li level scheme (not to scale) showing the D_2 and D_1 hyperfine structure and the transitions used for the D_2 MOT and the D_1 molasses. The laser detuning from the repumper and cooling transitions of the D_1 molasses are δ_1 and δ_2, respectively, while their relative detuning is δ.

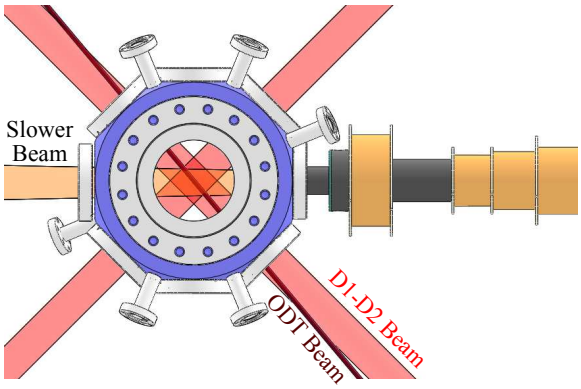

Figure 3. Top view of the science chamber, showing the configuration of the D_2 MOT/D_1 molasses beams, the Slower beam and the ODT beam.

3. D_1 gray-molasses cooling

We characterize the D_1 gray-molasses by measuring the temperature T and and the number of atoms N as a function of different parameters. T and N, after 2 ms in the molasses, are determined by time-of-flight (TOF) measurements, using absorption imaging resonant with the D_2 transition. In Fig. 4 (a) the values of T and the molasses capture efficiency, defined as N/N_0, where $N_0 = 1.6\times10^9$ is the initial atom number, are reported as a function of the relative detuning $\delta = \delta_1 - \delta_2$, where δ_1 and δ_2 are the detuning of the D_1 repumper and cooling lasers from the $F = 1/2 \rightarrow F' = 3/2$ and $F = 3/2 \rightarrow F' = 3/2$ transitions, respectively (see Fig. 2). The detuning of the cooling light δ_2 is fixed at 5.4 Γ, and $I_{rep} = 0.18\ I_{cool}$, with $I_{cool} = 2.7\ I_S$. At the Raman resonance, i.e. $\delta = 0$, the temperature reaches its minimum value $T_{min} = 40.5(1.0)$ μK with a capture efficiency N/N$_0$ of 75 %, as a consequence of both Sisyphus cooling on the blue of the $F \rightarrow F' = F$ transition and the formation of a coherent dark state in a three level Λ-system [7–10]. Furthermore, the temperature dependence on δ, in a narrow range around the Raman resonance, exhibits an asymmetric Fano-profile, which is a signature of the occurrence of quantum interference [20]. For δ slightly blue-detuned from the resonance, a strong heating accompanied by a decrease of the capture efficiency is instead observed, as already discussed in Refs. [8, 9]. Out of the resonance, both T and N/N_0 reach stationary values due to the Sisyphus

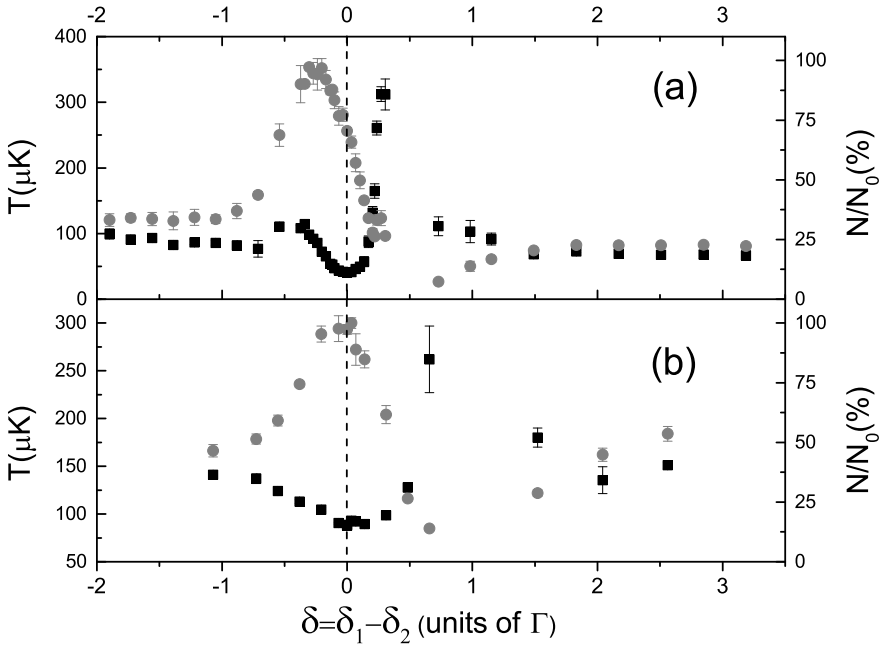

Figure 4. (a) Temperature T (black squares) and capture effciency N/N_0 (gray circles), with $N_0 = 1.6{\times}10^9$, as a function of the relative detuning δ. The laser intesities are: $I_{cool} = 2.7\ I_S$, $I_{rep} = 0.5\ I_S$ and $\delta_2 = 5.4\ \Gamma$. The molasses time is 2 ms. (b) Temperature T (black squares) and capture efficiency N/N_0 (gray circles), with $N_0 = 2{\times}10^7$, as a function of the relative detuning δ. The laser intesities are $I_{cool} = 2.7\ I_S$, $I_{rep} = 0.5\ I_S$ and $\delta_2 = 5.4\ \Gamma$. The molasses time is 300 μs and the ODT power is 120 Watt. In (a) and (b) the dotted vertical line indicates the value $\delta = 0$. Figures taken form Ref. [15].

effect alone. As the Raman condition is fulfilled, we find that the molasses efficiency is almost insensitive to δ_2 from a broad range of values from 3.5 to 8 Γ. This observation anticipates that the spatially varying AC Stark shift, due to the presence of the ODT, should not affect the D1 cooling mechanism, provided that the absolute detuning remains in this range. This is confirmed by our measurements of the D_1 light-shifts as a function of the trap intensity. Indeed, we find a differential Stark shift of about +2 Γ at the initial trap depth.

We directly verify the effectiveness of the gray-molasses in the presence of the ODT potential. The dipole trapping laser is turned on during the D_2 cooling stage, about 6 ms before switching to the D_1 light, and its power is ramped up to the maximum value in 5 ms. Mode-matching between the MOT and the optical trap is optimized by unbalancing the relative intensity of the MOT beams, in such a way to produce a cigar-shaped cloud perpendicular to the z-axis and elongated in the direction of the ODT beam. Despite this anisotropy, the performance of the gray-molasses is not substantially modified with respect to the balanced configuration. The number of atoms transferred into the ODT is maximized by applying a D_1 molasses cooling phase, lasting 2 ms, with δ=-0.2 Γ. This value corresponds to the maximum capture efficiency of the gray-molasses. In this way, we load into the optical potential about $2{\times}10^7$atoms at T=135(5) μK. In Fig. 4 (b), we show the Fano-profile recorded in the trap, 25 ms after the end of the ODT loading, by applying a further D_1 cooling stage lasting 300 μs. The molasses parameters are the same used in Fig. 4 (a). The dependence of T and N/N_0 on δ exhibits a behavior similar to the one observed in Fig. 4 (a). At δ=0, the temperature reaches its minimum value, $T_{min} = 80(5)$ μK, which is a factor 2 higher than that found in the absence of the trapping potential. This is accompanied by a broadening of the Fano-profile. This effect

can be ascribed to the large atomic density in the trap ($\sim 2\times10^{13}$ atoms/cm^3) which limits the D_1 cooling efficiency [14]. We observe that the molasses capture efficiency, corresponding to the minimum temperature, is 100 %. This is not surprising since now the initial temperature is low enough that all the atoms are cooled by the molasses. The optimal cooling strategy thus consists in a first D_1 phase, lasting 2 ms at δ=-0.2 Γ, followed by a second one, lasting 300 μs at δ=0. In this way, we first maximize the number of trapped atoms and then minimize their temperature. The last D_1 phase is followed by a 25 μs hyperfine pumping to the $|F = 1/2\rangle$ manifold, realized by turning off the D_1 repumper light before the cooling one. The hyperfine pumping increases the atomic temperature by about 10%.

4. Production of ^{6}Li quantum gases

To reach the quantum degenerate regime, we start the evaporative cooling of the two spin states $|F = 1/2, m_F = \pm1/2\rangle$, labeled as $|1\rangle$ and $|2\rangle$, at 840 G, close to the center of the Feshbach resonance [21]. After the hyperfine pumping stage, we ramp the magnetic field to the final value in about 30 ms and we decrease the trap laser power from 120 to 30 W in 500 ms. Multiple resonant radio-frequency sweeps create an incoherent balanced mixture of the $|1\rangle$ and $|2\rangle$ states. After this first evaporation ramp, we typically have 1×10^7 atoms per spin state at T$\simeq$ 30 μK. Molecular BECs are then produced by continuing the evaporation of $|1\rangle$-$|2\rangle$ mixture at 800 G, where the s-wave scattering length a_{12} is of the order of 11000 a_0 [21], with a_0 being the Bohr radius. The temperature T and the total number of atoms N as a function of the evaporation time are shown in Fig. 5 (a).

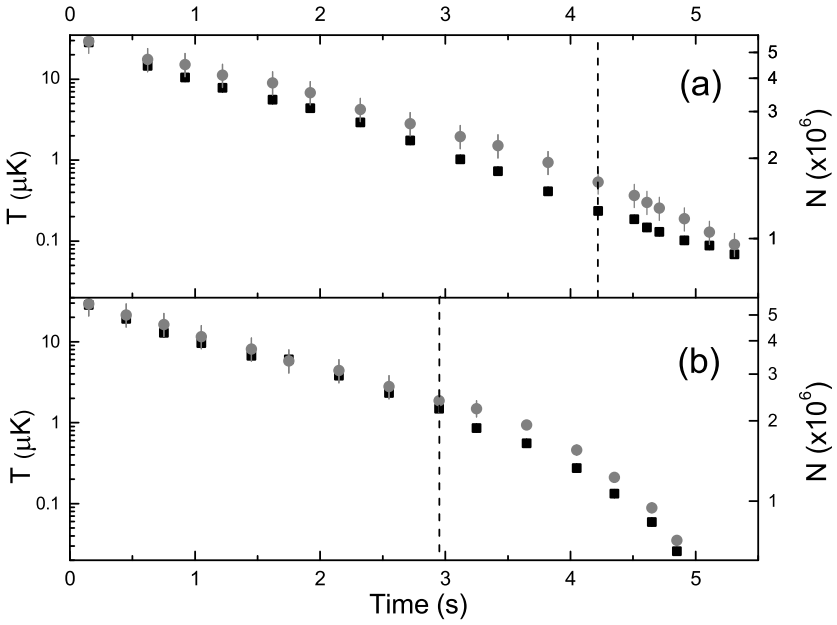

Figure 5. (a) Temperature T (black squares) and total atom number N (gray circles) as function of time during forced evaporation in the ODT at B=800 G. The dotted vertical line indicates the evaporation time for which T/T$_c$=1. (b) Temperature T (black squares) and total atom number N (gray circles) as function of time during forced evaporation in the ODT at B=300 G. The dotted vertical line indicates the evaporation time for which T/T$_F$=1. Figures taken form Ref. [15].

At a magnetic field of 800 G, molecules are formed via three-body recombination when

the temperature of the sample becomes lower than the molecular binding energy. At T=T$_c$=210(20) nK, we observe the onset of condensation for $N_{mol} \simeq 1 \times 10^6$ molecules. To image the molecular cloud in time of flight, we adiabatically sweep the magnetic field to 690 G to reduce the inter-particle interaction. At T$_c$, the radial trap frequencies are $2\pi\times239(2)$ Hz (along the z-axis) and $2\pi\times111(3)$ Hz and the axial frequency, given by the magnetic curvature of our Feshbach coils, is $2\pi\times8.2(1)$ Hz. By further reducing the trap depth, we observe the formation of an almost pure mBEC of about $N_{mol} \simeq 5 \times 10^5$. The same method is used to produce a unitary Fermi Gas at the Feshbach resonance. We observe ultracold clouds of about 2×10^6 particles at a temperature corresponding to T$_c$, when sweeping to the BEC side.

We follow a slightly different strategy for producing weakly-interacting Fermi gases. In this case, we evaporate the $|1\rangle$-$|3\rangle$ spin-mixture, where the $|3\rangle$ state corresponds to the $|F = 3/2, m_F = -3/2\rangle$ state at low magnetic fields. The mixture is created at T$\simeq$30 μK by transferring 100% of the atoms from the state $|2\rangle$ to the $|3\rangle$ by a radio-frequency sweep. The mixture is then evaporated at 300 G, where the $|1\rangle$-$|3\rangle$ s-wave scattering length is $a_{13} \simeq -880a_0$, about three times larger than $a_{12} \simeq -290a_0$ [21], strongly enhancing the evaporation efficency. The axial confinement, at this magnetic field, is provided by a magnetic curvature generated by an additional pair of coils. In Fig. 5 (b), we report the evaporation trajectory for the $|1\rangle$-$|3\rangle$ mixture at 300 G. This trajectory is similar to the one reported in Fig. 5 (a), showing the efficient thermalization of the $|1\rangle$-$|3\rangle$ mixture. After 3 seconds of forced evaporation, the system enters the degenerate regime with $N_{|1\rangle}$=$N_{|3\rangle}$=2×10^6 atoms. After a further 2 seconds, we produce a highly degenerate Fermi gas of $N_{|1\rangle}$=$N_{|3\rangle}$=3.5×10^5 atoms at $T/T_F \simeq 0.06(1)$, where T$_F$ is the Fermi temperature defined as $k_B T_F = \hbar\varpi(6N_i)^{1/3}$, where ϖ is the mean trap frequency. Here, we measure radial trapping frequencies of $2\pi\times231(3)$ Hz (along the z-axis) and $2\pi\times111.5(2)$ Hz, and an axial trapping frequency of $2\pi\times12.4(1)$ Hz.

5. High-resolution imaging and production of a thin optical barrier

We implement an optical setup, along the vertical direction, both for high-resolution imaging and for producing engineered optical potentials. In particular, we describe how to create and imprint on the atomic cloud a green sheet of light. The main component of our system is an aspheric lens [22] with a diameter of 45 mm and a focal length of 32 mm, placed at a few millimeters from the upper reentrant viewport (see Fig. 6 (a)). The lens has a numerical aperture of 0.61 which corresponds to a theoretical resolution of $\sim\lambda$, thus approaching the diffraction limit. The absorption imaging and the vertical MOT beams, which have linear orthogonal polarizations, are superimposed, using a polarization beam splitter, then they are circularly polarized with opposite sign by a $\lambda/4$ waveplate and sent through the chamber via the lower reentrant viewport. In order to retro-reflect back the incoming MOT beam, we place after the aspheric lens in close sequence a $\lambda/4$ waveplate and a wire-grid polarizer (WGP). The relative optical axis between the $\lambda/4$ waveplate and the WGP is adjusted in a such way that the MOT beam is reflected back whereas the imaging beam is transmitted. All the optical elements are assembled together in a custom-designed holder, made with PEEK polymer, which is, in turn, aligned using a five-axis optical positioner. The laser light used to produce the optical barrier is provided by a 532 nm Nd:YVO4 laser. A 532 nm beam, after crossing a cylindrical lens with a focal length of 200 mm, is overlapped to the imaging beam, coming from the bottom, by means of a dichroic mirror. Then, the green beam, which is properly linearly polarized, is transmitted by the WGP and is focused by the aspheric lens on the atomic sample. This configuration produces a repulsive sheet of light with waists of about 2 μm (along the longitudinal axis of the ODT)x850 μm (see Fig. 6 (b)). The minimum value of the axial waist is limited by residual aberrations as well as diffraction effects introduced by the optical components. The green barrier added to the optical dipole trap potential produces a double-well potential landscape for the atoms. As preliminary result, we show in Fig. 7 the in-situ absorption image, recorded by a CCD camera, and the

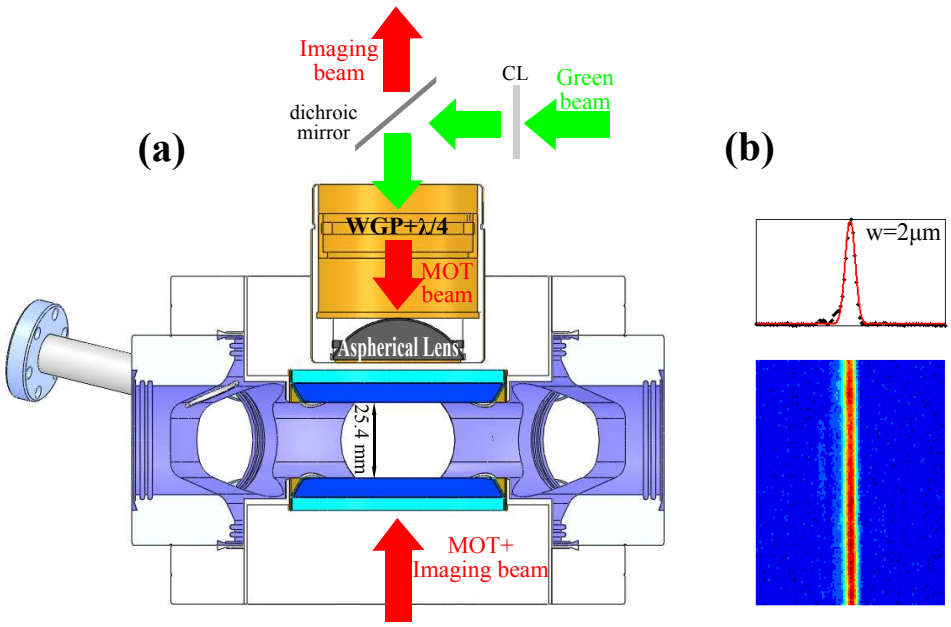

Figure 6. (a) Optical system for high-resolution imaging and production of a repulsive like-sheet potential. The vertical MOT beam is retro-reflected back by a wire-grid polarizer (WGP) and a $\lambda/4$ waveplate. The 670 nm imaging beam and the 532 nm beam are superimposed using a dichroic mirror. By combining a cylindrical lens (CL) and the objective (aspheric lens), we create a thin optical barrier for the atoms. (b) Intensity profile of the 532 nm beam, after the cylinrical lens, projected by the obective on a CCD camera.

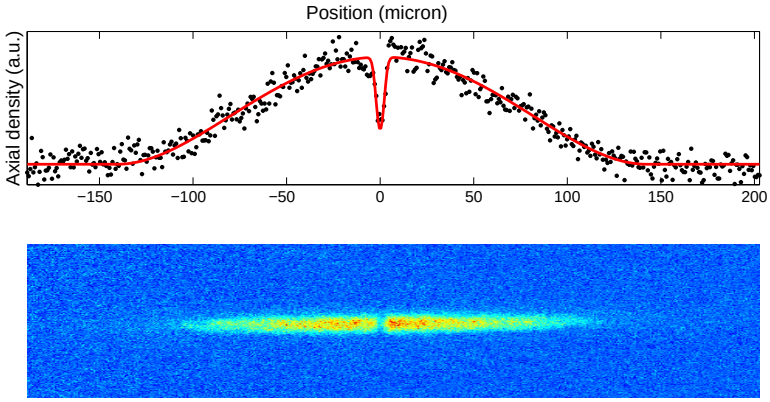

Figure 7. In-situ absorption image of a mBEC at 690 G (bottom panel) and its axial density profile (top panel) in a double-well potential formed by the superposition of the ODT trap potential and a green barrier with a size of about 2 μm. The density profile has been fitted by a sum of a Thomas-Fermi function and a Gaussian peak (red curve).

relative axial density profile of a mBEC (produced following the procedure described in Sec. 4) of about 1.2×10^4 molecules at 690 G in the double-well trap. The atomic density distribution has been determined using the absorption imaging along the z-axis. The power of the green beam on the atomic cloud is about 2 mW.

In the future, we plan to investigate the coherent oscillations between two fermionic superfluids across the barrier. Although the Josephson effect in weakly linked Bose-Einstein condensates has been theoretically described [23] and experimentally observed [24–26], much less is known about its fermionic counterpart. Recently, several theoretical papers have investigated the tunneling dynamics of both fermionic superfluids [27–29] and spin-polarized Fermi gases [30, 31] through a barrier. Our setup allows to address all these regimes by simply tuning the atomic scattering length across the Feshbach resonance. The case of a Fermi gas at unitarity is of special interest since all scales are set by the inverse of the Fermi wave vector k_F. In our typical experimental conditions k_F^{-1} is of the order of 0.5 μm; therefore, the coherence length $l_{coh}{\sim}k_F^{-1}$ is still comparable with the barrier size, allows for testing of different theoretical approches.

6. Conclusion

In conclusion, we have demonstrated an all-optical method for fast and efficient production of quantum gases of ^{6}Li, without the need of any additional coolant atomic species [32]. Our scheme is based on a D_1 gray-molasses phase which provides sub-Doppler cooling with a high capture efficiency. This ensures an efficient transfer into an ODT, where we evaporate down to the degenerate regime. We observe that the D_1 cooling also works in the presence of a deep optical dipole potential. This result suggests the possibility to exploit this scheme to image ^{6}Li atoms in optical lattices with single-site resolution [33, 34]. In an experimental run, lasting 11 s, we produce either mBECs and crossover superfluids of $5{\times}10^5$ dimers/pairs or binary mixtures of degenerate Fermi gases of $3.5{\times}10^5$ atoms per spin state at $T/T_F < 0.1$.

We have also developed, and integrated in our setup, a simple optical system for both high-resolution imaging and for creating a thin optical barrier. We have then verified that this system allows us to produce and imprint on the atomic cloud a green barrier with a size of about 2 μm. As this repulsive well is added to the harmonic potential, generated by our optical trap, an effective double-well potential is created. We plan to study the tunneling dynamics of two quantum gases of ^{6}Li in the double-well trap, starting from the BEC regime of composite molecules reaching the BEC-BCS crossover. This represents the first step towards the experimental realization of a Josephson junction with ultracold Fermi gases.

Acknowledgments

We would like to thank the technical staff of LENS for assistance. Special acknowledgments to the LENS Quantum Gases group. This research was supported under the European Research Council Grant No. 307032 QuFerm2D and the European Council Advanced Grant No. 247371 DISQUA.

References

[1] I. Bloch, J. Dalibard, and W. Zwerger, Rev. Mod. Phys. **80**, 885 (2008).
[2] Proceedings of the International School of Physics Enrico Fermi, Course CLXIV, Edited by M. Inguscio, W. Ketterle, and C. Salomon, 2007, IOS Press Amsterdam.
[3] M. D. Barrett, J. A. Sauer, and M. S. Chapman, Phys. Rev. Lett. **87**, 010404 (2001).
[4] K. M. O'Hara, S. L. Hemmer, M. E. Gehm, S. R. Granade, and J. E. Thomas, Science **298**, 2179 (2002).
[5] S. Jochim, M. Bartenstein, A. Altmeyer, G. Hendl, S. Riedl, C. Chin, J. Hecker Denschlag, and R. Grimm, Science **302**, 2101 (2003).
[6] J. Dalibard and C. Cohen-Tannoudjii, J. Opt. Soc. Am. B **6**, 2023 (1989).
[7] D. Rio Fernandes, F. Sievers, N. Kretzschmar, S. Wu, C. Salomon, and F. Chevy, Europhys. Lett. **100**, 63001 (2012).
[8] A. T. Grier, I. Ferrier-Barbut, B. S. Rem, M. Delehaye, L. Khaykovich, F. Chevy, and C. Salomon, Phys. Rev. A **87**, 063411 (2013).
[9] D. Nath, R. K. Easwaran, G. Rajalakshmi, and C. S. Unnikrishnan, Phys. Rev. A **88**, 053407 (2013).
[10] G. Salomon, L. Fouch, P. Wang, A. Aspect, P. Bouyer, and T. Bourdel, Europhys. Lett. **104**, 63002 (2013).
[11] G. Grynberg and J. -Y. Courtois, Europhys. Lett. **27**, 41 (1994).

[12] M. Weidemüller, T. Essingler, M. A. Ol'shanii, A. Hemmerich, and T. W. Hänsch, Europhys. Lett. **27**, 109 (1994).
[13] D. Boiron, C. Triché, D. R. Meacher, P. Verkerk, and G. Grynberg, Phys. Rev. A **52**, R3425 (1995).
[14] D. Boiron, A. Michaud, J. M. Fournier, L. Simard, M. Sprenger, G. Grynberg, and C. Salomon, Phys. Rev. A **57**, R4106 (1998).
[15] A. Burchianti, G. Valtolina, J. A. Seman, E. Pace, M. De Pas, M. Inguscio, M. Zaccanti, and G. Roati, Phys. Rev. A **90**, 043408 (2014).
[16] F Sievers, S Wu, N Kretzschmar, DR Fernandes, D Suchet, M Rabinovic,C V Parker, L Khaykovich, C Salomon, F Chevy, arXiv:1410.8545 (2014).
[17] P. M. Duarte, R. A. Hart, J. M. Hitchcock, T. A. Corcovilos, T.-L. Yang, A. Reed, and R. G. Hulet, Phys. Rev. A **84** ,061406R (2011).
[18] D. C. McKay, D. Jervis, D. J. Fine, J. W. Simpson-Porco, G. J. A. Edge, and J. H. Thywissen, Phys. Rev. A **84**, 063420 (2011).
[19] J. Sebastian, C Gross, K Li, H. C. J. Gan, W Li and K. Dieckmann, Phys. Rev. A **90**, 033417 (2014).
[20] B. Lounis and C. Cohen-Tannoudji, J. Phys. II France **2**, 579 (1992).
[21] G. Zürn, T. Lompe, A. N. Wenz, S. Jochim, P. S. Julienne, and J. M. Hutson, Phys. Rev. Lett. **110**, 135301 (2013).
[22] A similar optical scheme has been developed by the Jochim group in Heidelberg.
[23] A. Smerzi, S. Fantoni, S. Giovanazzi, and S. Shenoy, Phys. Rev. Lett. **79**, 4950 (1997).
[24] F. S. Cataliotti, S. Burger, C. Fort, P. Maddaloni, F. Minardi, A. Trombettoni, A. Smerzi, and M. Inguscio, Science **293**, 843 (2011).
[25] M. Albiez, R. Gati, J. Fölling, S. Hunsmann, M. Cristiani, and M. K. Oberthaler, Phys. Rev. Lett. **95**, 4950 (2005).
[26] S. Levy, E. Lahoud, I. Shomroni, and J. Steinhauer, Nature **449**, 579 (2007).
[27] A. Spuntarelli, P. Pieri, and G.C. Strinati, Phys. Rev. Lett. **99**, 040401 (2007).
[28] P. Zou and F. Dalfovo, arXiv:1401.2007v1 (2014).
[29] F. Ancilotto, L. Salasnich, and F. Toigo, Phys. Rev. A **79**, 033627 (2009).
[30] L. Salasnich, G. Mazzarella, M. Salerno, and F. Toigo, Phys. Rev. A **81**, 023614 (2010).
[31] T. Macrì and A. Trombettoni, Laser Phys. A **81** 23, 095501 (2013).
[32] Z. Hadzibabic, S. Gupta, C. A. Stan, C. H. Schunck, M. W. Zwierlein, K. Dieckmann, and W. Ketterle, Phys. Rev. Lett. **91**, 160401 (2003).
[33] W. S. Bakr, J. I. Gillen, A. Peng, S. Fölling, and M. Greiner, Nature **462**,74 (2009).
[34] J. F. Sherson, C. Weitenberg, M. Endres, M. Cheneau, I. Bloch, and S. Kuhr, Nature **467**, 68 (2010).